


## Research Article

# Sugarcane Bagasse-Derived Cellulose Nanocrystal/Polyvinyl Alcohol/Gum Tragacanth Composite Film Incorporated with Betel Leaf Extract as a Versatile Biomaterial for Wound Dressing

Luong Ngoc Diem,<sup>1</sup> Selorm Torgbo ,<sup>1</sup> Indranil Banerjee,<sup>2</sup> Kunal Pal ,<sup>3</sup>  
Udomlak Sukatta,<sup>4</sup> Prapassorn Rugthaworn,<sup>4</sup> and Prakrit Sukyai <sup>1,5</sup>

<sup>1</sup>Cellulose for Future Materials and Technologies Special Research Unit, Department of Biotechnology, Faculty of Agro-Industry, Kasetsart University, Chatuchak, Bangkok 10900, Thailand

<sup>2</sup>Department of Bioscience and Bioengineering, Indian Institute of Technology Jodhpur, NH-65 Karwar, Jodhpur 342037, India

<sup>3</sup>Department of Biotechnology and Medical Engineering, National Institute of Technology, Rourkela, Odisha 769008, India

<sup>4</sup>Kasetsart Agriculture and Agro-Industrial Product Improvement Institute, Kasetsart University, Bangkok 10900, Thailand

<sup>5</sup>Center for Advanced Studies for Agriculture and Food (CASAF), Kasetsart University Institute for Advanced Studies, Kasetsart University, Chatuchak, Bangkok 10900, Thailand

Correspondence should be addressed to Prakrit Sukyai; [fagipks@ku.ac.th](mailto:fagipks@ku.ac.th)

Received 28 March 2023; Revised 21 June 2023; Accepted 1 July 2023; Published 13 July 2023

Academic Editor: Swarup Roy

Copyright © 2023 Luong Ngoc Diem et al. This is an open access article distributed under the Creative Commons Attribution License, which permits unrestricted use, distribution, and reproduction in any medium, provided the original work is properly cited.

In this study, nanocomposite film was fabricated using cellulose nanocrystals (CNCs) as nanofiller in a polymer matrix of polyvinyl alcohol (PVA) and gum tragacanth (GT) via solution casting. CNCs were extracted from sugarcane bagasse using a steam explosion technique followed by acid hydrolysis. Initial analysis of CNCs by transmission electron microscopy (TEM) showed nanosized particles of 104 nm in length and 7 nm in width. Physical and chemical characteristics of neat PVA, PVA/GT, and PVA/GT/CNC films with varying concentrations of CNCs (from 2% to 10%) were analyzed by the scanning electron microscopy (SEM), Fourier transform infrared (FTIR) spectrometry, mechanical test, and swelling test. The SEM analysis showed cluster formation of CNCs in the polymer matrix at high concentration. The developed films were transparent. FTIR spectrometry analysis confirmed the chemical functional groups of the various components in the film. The presence of GT and CNCs in the polymer matrix improved the characteristics of films as evident in the prolonged stability for 7 days and increased mechanical properties. The highest elastic modulus of  $1526.11 \pm 31.86$  MPa and tensile strength of 80.39 MPa were recorded in PVA/GT/CNC2 film. The swelling ability, however, decreased from 260% to 230%. Cytotoxicity analysis of the PVA/GT/CNC film showed that it is nontoxic to mouse fibroblast cells L929 with 95% cell viability. Films loaded with betel leaf extract exhibited excellent antibacterial activities against *Staphylococcus aureus* DMST 8840 and *Pseudomonas aeruginosa* TISTR 781 with  $28.20 \pm 0.84$  mm and  $23.60 \pm 0.55$  mm inhibition zones, respectively. These results demonstrate that PVA/GT/CNC loaded with the betel leaf extract could act as promising and versatile wound dressings to protect the wound surface from infection and dehydration.

## 1. Introduction

Natural and synthetic polymers have been investigated over the years as biomaterials for biomedical applications [1, 2]. To blend natural polymers with synthetic ones is another unique way of preparing versatile polymeric materials for biomedical applications [3]. The synthetic polymers have

good mechanical properties and thermal stability; however, they can inhibit cell growth due to residue of initiators and other compounds. Natural polymers on the other hand are usually biodegradable, biocompatible, and bioactive in nature [3–5]. Polyvinyl alcohol (PVA) is a linear synthetic polymer which is nontoxic, biocompatible, thermostable, and water-soluble with film forming properties [6, 7]. PVA

has been used as the main matrix with outstanding physical and chemical properties in biomedical applications [8, 9]. However, the scope of PVA application is limited by its instability, insufficient elasticity, and lack of cell-specific bioactivities [9, 10]. To tackle these problems, several attempts have been made by incorporating substances such as chitosan [11, 12], dextran [13], polyion liquid [14], and nanocellulose [15, 16]. PVA-based composite films containing bacterial cellulose and epsilon polylysine [16], dextran aldehyde hydrogel [13], and silk fibroin-PVA composite film coated with chitosan-ZnO nanoparticles [17] were reported for wound dressings. These dressings demonstrated good absorbability and tissue regeneration with low cytotoxicity and inhibited bacterial infections with enhanced mechanical properties. However, these materials lacked essential features such as good swelling properties and mediated angiogenesis.

Gum tragacanth (GT) comprises a complex mixture of highly branched heterogeneous hydrophilic polysaccharides mainly D-galacturonic acid and other sugar units with numerous functional groups that provide a suitable medium for cell growth and mediated angiogenesis [18–20]. GT is one of the most abundant and renewable natural raw materials. GT is readily accessible, relatively affordable, nontoxic, biocompatible, environmentally friendly, and widely used in biomedical science [21]. As a natural polysaccharide, GT has been applied in various biotechnological industries [19]. GT has been incorporated into PVA for application in drug delivery [22, 23], scaffold for skin substitutes [24], and wound dressing [25–27]. High degradation ability, stability against microbial, and heat in the living systems have triggered several studies on GT for wound dressings [21]. A bio-based wound dressing made with gelatin, gum Arabic, and polyurethane was also reported for wound care application [28]. In a related study, PVA and Iranian gum tragacanth (IGT) biocomposite with nanoclay was reported to have superior degradation and higher chemical and mechanical stability for wound dressing [29]. In addition, GT also serves as a suitable stabilizing agent for biosynthesis of nanoparticles [30]. The major limitation of GT in biomedical application has to do with its rapid degradation, which affects the mechanical and biological properties. Interestingly, this drawback can be overcome using nanofillers such as cellulose nanocrystals.

Large amount of waste is unfortunately generated from sugarcane processing industries, which composed mainly of bagasse, molasses, filter cake, and leaves [31–33]. The bagasse and leaves are rich in cellulose fibers for nanocellulose production. Cellulose nanocrystals (CNCs) are potential reinforced nanofillers with needle-like shapes ranging from 100 nm to 250 nm in length and from 5 nm to 70 nm in width, high aspect ratio, and high crystallinity [34]. Dispersion of CNCs in synthetic polymers will provide good mechanical properties due to their unique crystalline domains with inherent stability that contributes stiffness and elasticity to the material [35]. CNCs have zero or low toxicity and can stimulate long-term cell proliferation [36]. Hence, CNCs have been applied in various aspects of medical fields [37]. The addition of CNC into carboxymethyl cellulose-

glycerol (CMC-G) matrix was reported to improve the physicochemical properties and stability of the film [38]. A study on bioactive wound dressing using hyaluronic acid-(HA-) based nanofibers with PVA revealed that incorporating CNCs into PVA/HA significantly improved swelling and mechanical properties [39]. However, it lacks antimicrobial properties. Antimicrobial activity is an important factor for considering biomaterials for wound dressings. This prevents contamination or bacterial infection while improving the healing process. For that matter, plant-based bioactive compounds are widely used as an antibacterial agent in wound dressings [40, 41]. An alternative nanocomposite film for traditional wound dressing incorporated with black pepper and ginger essential oils was reported to significantly inhibit the growth of bacteria [42]. In a related study, papain immobilized in bacterial cellulose as a polymer template was reported for wound dressing with strong antibacterial action [43]. Plant extractive from betel leaf (*Piper betle* L.) was used in this study. Betel leaf is a traditional herbal medicine commonly found in Southeast Asia and East African countries that contains phenolics, flavonoids, alcohols, alkaloids, terpenes, fatty acids, and organic acids [44, 45]. These compounds were reported to exhibit several biological properties including antibacterial, antifungal, anti-inflammatory, and antioxidant activities [45–48].

Different treatment strategies and dressings with special properties are required to regenerate damaged tissues in wound management. Wound dressing material should fully cover the affected area, create conducive environment to prevent contamination, and have the ability to absorb exudates on the wound surface. In addition, it must degrade rapidly, be easy to change without causing pain or trauma at the wound bed, be nontoxic, and be cost effective [49, 50]. Film dressings are mostly preferred for superficial injuries to protect skin prone to abrasion or external contamination [50]. The transparency of film allows daily observation without its removal and prevents damage to the wound bed [49]. Therefore, combination of different polymers impregnated with the plant extract could act as novel film with unique properties for biomedical consideration in wound dressings.

Herein, PVA, GT, and CNCs were used to produce a versatile film for wound dressing. The physicochemical characteristics of the composite films which are essential for wound dressing were evaluated. Biological properties of PVA/GT/CNC were examined for the film's ability to support cell viability. The ability of the film to prevent bacterial infection was examined by loading the crude betel leaf extract as an antimicrobial agent. A preprint has previously been published [51].

## 2. Materials and Methods

**2.1. Materials.** Sugarcane bagasse was obtained from Mitr Phol Sugar Corporation., Ltd. (Klongteoy, Thailand). The chemical reagents including sodium chlorite ( $\text{NaClO}_2$ ), glacial acetic acid ( $\text{CH}_3\text{COOH}$ ), and sulfuric acid 98% ( $\text{H}_2\text{SO}_4$ ) were purchased from Ajax Finechem Pty., Ltd.

(New Zealand), Merck (Darmstadt, Germany), and QReC (New Zealand), respectively. Acetone ( $C_3H_6O$ ) was supplied by RCL Labscan Limited (Bangkok, Thailand). Polyvinyl alcohol (PVA) ( $M_w = 89,000\text{--}98,000$ ) from EMD Millipore Corporation (Germany). All other reagents used were of analytical grade.

### 2.2. Nanocellulose Extraction from Sugarcane Bagasse (SCB).

The SCB was dried at  $55^\circ\text{C}$  for 24 h and then treated by steam explosion (Nitto Koatsu, Japan) at  $190^\circ\text{C}$  with a pressure of 13 MPa for 15 min [52]. The exploded sample without sugar-rich liquid fraction was bleached by treating with 1.4% w/w sodium chlorite ( $\text{NaClO}_2$ ) solution, which was adjusted to pH of 4.0 with glacial acetic acid ( $\text{CH}_3\text{COOH}$ ) at  $70^\circ\text{C}$ . Bleaching chemicals were added every hour until the sample turned white. The bleached sample was then filtered and washed several times until the pH was neutral [53, 54]. The dried bleached cellulose fibers were dispersed in 64% w/v  $\text{H}_2\text{SO}_4$  at a solid-to-liquid ratio of 1:20 with constant stirring at 500 rpm for 75 min at  $45^\circ\text{C}$ . The hydrolysis reaction was stopped using cold deionized (DI) water and centrifugation was repeated at 15,000 rpm for 15 min at  $4^\circ\text{C}$ . The supernatant was removed and replaced by clean DI water, followed by dialysis to obtain CNCs. The CNC was sonicated (Bransonic Model 2201R-MT, USA) and kept at  $4^\circ\text{C}$  for further use.

**2.3. Preparation of Composite Films.** An aqueous solution of PVA (10% w/v) was prepared under continuous stirring at  $80^\circ\text{C}$  and, 10% w/w of GT based on a specific amount of PVA was added to create PVA/GT solution [10]. The CNC composite film was fabricated by adding CNC suspension with varying concentrations (2% to 10%) to PVA/GT solution, denoted as PVA/GT/CNC2 to PVA/GT/CNC10. The mixture was stirred for 30 min to obtain a homogenous state before pouring into Petri dishes and dried at  $37^\circ\text{C}$  for 48 h. The dried films were soaked in crude betel leaf extract prepared in propylene glycol (PG) at different concentrations (2%, 3%, and 4% w/v) for 24 h and dried at  $37^\circ\text{C}$  as an antimicrobial agent.

**2.4. Transmission Electron Microscopy (TEM).** Dimension of CNC particles was examined by TEM (Hitachi Model HT7700, Japan). Briefly, 0.01% w/v CNC suspension was deposited on a carbon-coated copper grid, poststained with 2% w/v uranyl acetate solution and dried for 8 min. The sample was analyzed with an accelerating voltage of 100 kV [55]. CNC dimensions were determined using the ImageJ program.

**2.5. Optical and Transparency Measurement.** Film transparency was determined using a Genesys 10S UV-Vis spectrophotometer (Thermo Fisher Scientific, USA) at a wavelength of 560 nm [56]. Film specimens were cut into rectangular shapes ( $2 \times 40$  mm) and placed inside the spectrophotometer cells. An empty spectrophotometer cell was set as a blank. All measurements were conducted in

triplicate and the percentage of film transparency was calculated using the following equation [57]:

$$\text{percentage transparency (\%T)} = \left( \frac{T_f}{T_b} \right) \times 100, \quad (1)$$

where  $T_f$  and  $T_b$  are the transmittance values of the film sample and blank cell, respectively.

**2.6. Scanning Electron Microscopy (SEM).** Surface and cross section of the composite films were investigated by SEM (Hitachi Model, Joel JSM5600LV, Japan) with an accelerating voltage of 15–20 kV [31]. To observe the cross section, film specimens were freeze-cracked following immersion in liquid nitrogen. Each piece was deposited on a cylindrical holder and coated with a thin gold layer (5–10 nm thickness) before observation.

### 2.7. Fourier Transform Infrared (FTIR) Spectrometry Analysis.

The PVA/GT/CNC composite films were cut into  $10 \times 10$  mm squares at random locations. Infrared spectra of each sample were recorded using an FTIR (Bruker Tensor 27 Spectrometer, USA) in the range of  $4000\text{--}500\text{ cm}^{-1}$  with a resolution of  $4\text{ cm}^{-1}$  in attenuated total reflection (ATR) mode.

**2.8. Swelling Ratio and Stability.** Swelling ratio and stability of the composite films were evaluated based on the amount of water absorbed and percentage of weight loss in 7 days, respectively. Briefly, dried film specimens ( $15 \times 15$  mm) were immersed in DI water at ambient temperature. For each turn of measurement [58], swelling ratio was assessed by taking the weight of swollen samples. To examine the stability of composite films, the swollen samples were taken and dried again to determine the difference in dried weight before and after immersion. All samples were weighed by an analytical balance in triplicate. The results were calculated using the following equations [13]:

$$\text{swelling ratio (\%)} = \frac{(M_1 - M_0)}{M_0} \times 100, \quad (2)$$

$$\text{weight loss (\%)} = \frac{(M_0 - M_1)}{M_0} \times 100, \quad (3)$$

where  $M_0$  and  $M_1$  represent sample weight before and after immersion, respectively.

**2.9. Mechanical Properties.** Tensile strength and elongation at break of the composite films were evaluated using a universal testing machine (AGS-J 1 kN, Japan) according to the ASTM D882-02 standard method. Briefly, the films were cut into rectangular shapes ( $10 \times 50$  mm) and kept at  $25^\circ\text{C}$  with relative humidity of  $50\% \pm 2\%$  until reaching constant weight. The films were tightly fixed in the grips with 30 mm initial space and pulled apart by a 1 kN load cell. The experiment was conducted in triplicate. The tensile strength

and elongation at break were calculated from the following equations, respectively [57]:

$$\text{tensile strength} = \frac{F}{(T \times W)}, \quad (4)$$

where  $F$ ,  $T$ , and  $X$  are the maximum force, film thickness, and width of film, respectively.

$$\text{Elongation at break} = (D_1 - D_0) \times 100, \quad (5)$$

where  $D_1$  is the distance of rupture and  $D_0$  is the initial distance between grips.

**2.10. Cytotoxicity.** Cytotoxicity test was conducted using the colorimetric assay which is based on the ability of the cells (cellular oxidoreductase enzymes) to reduce the tetrazolium dye 3-(4,5-dimethylthiazol-2-yl)-2,5-diphenyltetrazolium bromide (MTT) to its insoluble formazan, following the ISO 10993-5 standard [59]. Mouse fibroblast cells L929 (NCTC clone 929: CCL1 from the American Type Culture Collection (ATCC), strain L) were cultured in minimum essential medium (MEM) with an appropriate cell density of  $10^5$  cells/ml and incubated for  $24 \pm 2$  h. The films were sterilized by UV irradiation for 15 min, prepared at  $3 \text{ cm}^2/\text{ml}$ , and extracted for  $24 \pm 2$  h at  $37 \pm 1^\circ\text{C}$ . The extracts were further incubated for  $24 \pm 2$  h before being stained with MTT assay for 2 h. A Thermanox (Nunc) coverslip was used as the negative control, while polyurethane film containing 0.1% zinc diethyldithiocarbamate served as the positive control. After culturing with fibroblast cells for 24 h, tested samples were compared to the negative and positive controls. A microplate reader was used to determine cell viability at absorbance of 570 nm using equation (6) [25]. Cell viability above 70% from equation (6) was considered noncytotoxic.

$$\text{Cell viability} = \frac{\text{OD}_{\text{sample}}}{\text{OD}_{\text{blank}}} \times 100\%, \quad (6)$$

where  $\text{OD}_{\text{sample}}$  and  $\text{OD}_{\text{blank}}$  are measurements of optical density of the test sample and blank sample, respectively.

**2.11. Antimicrobial Ability.** Antimicrobial property of the films loaded with the crude betel leaf extract was studied against *Staphylococcus aureus* DMST 8840 and *Pseudomonas aeruginosa* TISTR 781 using the agar diffusion method. Before the experiment, *S. aureus* and *P. aeruginosa* suspensions of  $10^6$  CFU/ml were evenly spread over nutrient agar plates. Films loaded with the betel leaf extract were placed on an inoculated agar surface, with paper discs loaded with erythromycin used as the positive control and PG as the negative control. The culture plates were incubated at  $37^\circ\text{C}$  for 18 h, and the inhibition zone was measured at the end of the incubation time using digital Vernier caliper [60].

**2.12. Statistical Analysis.** The statistical analysis of data was done by one-way analysis of variance (ANOVA) at a confidence level of 0.05 using the Minitab program. All data

were expressed as mean  $\pm$  standard deviation. A  $p$  value  $< 0.05$  was considered statistically significant.

### 3. Results and Discussion

**3.1. Characterization of Nanocellulose.** SCB (Figure 1(a)) consists of cellulosic and noncellulosic components. A series of treatment steps are involved in removing the non-cellulosic components (hemicellulose and lignin) to promote defibrillation. Removal of major noncellulosic components increased the cellulose content (Figure 1(b)). The bleached fiber was subsequently subjected to acid hydrolysis that caused disordering in the glycosidic linkages and breakdown of the fibrous structures. These resulted in the reduction of fiber size to produce CNCs. The crystalline CNCs were presented as a stable colloidal suspension (Figure 1(c)). The surface of CNCs was linked to negatively charged particles of sulfate half ester groups derived from the acid hydrolysis process [35]. TEM analysis was carried out to determine particle size and distribution of CNCs. Results showed needle-like shapes of individual and aggregated particles (Figure 1(d)). Dimensions of the CNCs were approximately 104 nm in length and 7 nm in width, similar to sizes reported earlier [61, 62]. The stable colloidal property coupled with nanosize of particles make the CNCs an ideal candidate in composite film preparation.

#### 3.2. Characterization of Composite Film

**3.2.1. Optical Observation.** Table 1 shows the percentage transparency of the composite films. Neat PVA recorded the highest transmittance of  $91.27 \pm 0.43\%$  followed by PVA/GT at  $74.59 \pm 0.43\%$ . However, the incorporation of CNCs has drastically reduced the transparency of films. The PVA/GT/CNC10 film recorded the lowest transmittance of  $46.28 \pm 0.54\%$ . High significant difference ( $p < 0.05$ ) was recorded among PVA, PVA/GT, and PVA/GT/CNC composite films due to differences in light dispersion caused by the disparate viscosities of GT and PVA [63] and aggregation of CNCs as the concentration increased [64]. Optical properties also relate to the rearrangement in the internal structure of PVA molecules during the drying process [63, 65]. Although the opaqueness of films increased at higher CNC concentration (Table 1), visual observation showed they are all colorless and transparent (Figure 2). The film is ideal for wound dressings, as it will allow daily observation without its removal and prevents damage to the wound bed [49]. Optically transparent wound dressings offer an opportunity to monitor the wound healing progress without having to replace the dressing. In addition, the direct naked-eye observation is the most appropriate and effective way for detecting wound infection during the healing process [66, 67]. Films with the lowest and highest concentrations of CNCs were, therefore, selected for SEM analysis.

**3.2.2. SEM.** SEM micrograph (Figure 3) shows the surface and cross section of neat PVA, PVA/GT, and PVA/GT/CNC films. The neat PVA film had a uniform texture with

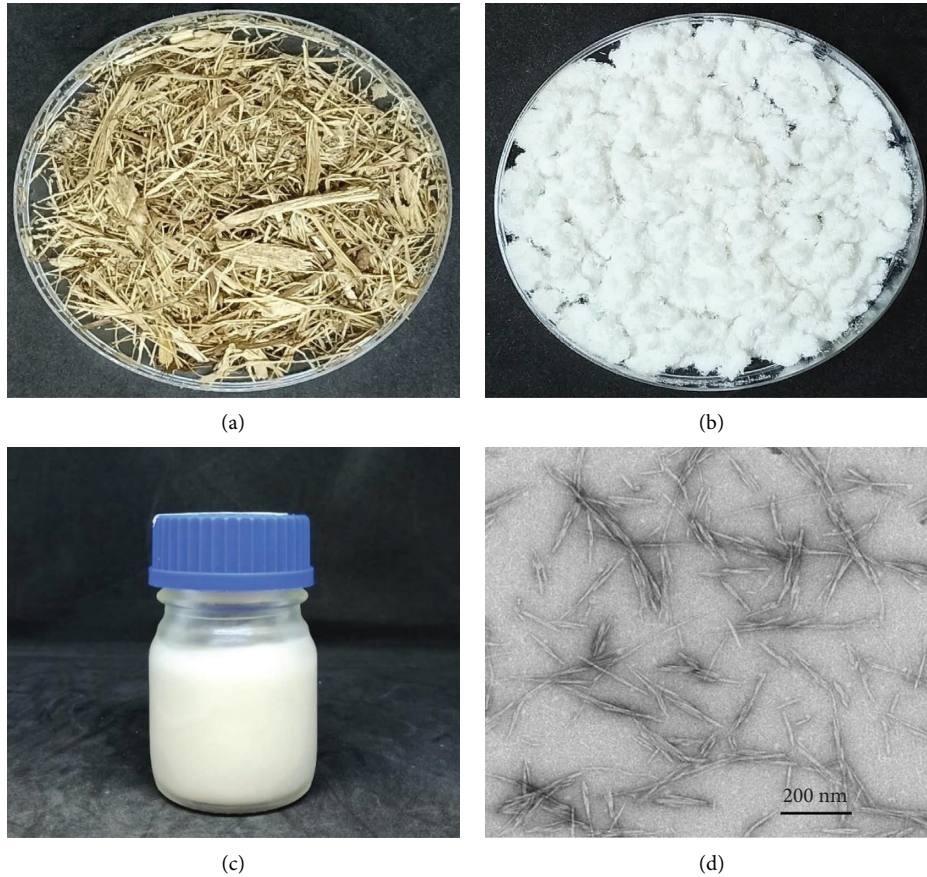


FIGURE 1: Photographs of (a) SCB, (b) bleached fiber, (c) CNCs, and (d) TEM image of CNCs.

TABLE 1: Transparency of PVA/GT composite films with different concentrations of CNCs.

Samples	Transmittance
PVA	$91.27 \pm 0.43^b$
PVA/GT	$74.59 \pm 0.43^c$
PVA/GT/CNC2	$74.30 \pm 0.17^c$
PVA/GT/CNC4	$68.94 \pm 0.11^d$
PVA/GT/CNC6	$68.79 \pm 0.11^d$
PVA/GT/CNC8	$59.70 \pm 0.39^e$
PVA/GT/CNC10	$46.28 \pm 0.54^f$
Control (blank)	$100 \pm 0.00^a$

For values with the same letter, the difference is not statistically significant, while different letters mean statistical significance ( $p \leq 0.05$ ).

a smooth planer surface and cross section (Figures 3(a) and 3(e)). However, the addition of GT changed the film surface to slightly rough, characterized by the presence of white dots on the surface and cracks in the cross section (Figures 3(b) and 3(f)). Mostafavi et al. [57] reported that the chemical structure of GT could organize into a more open and porous network [47]. Similarly, the film containing GT showed reduced homogeneous quality [65, 68]. Dispersion of CNCs in the PVA/GT films (Figure 3(c)) resulted in the disappearance of some white dots on the surface structure, suggesting that CNC particles filled in the polymeric matrix. Increasing the CNC content led to

assemblage and cluster formation of CNCs in the film (Figure 3(d)). This result agreed with a previous study by Jahan et al. [69]. The CNC particles were observed on the fractured shapes in the cross section (Figures 3(g) and 3(h)). The nanocellulose reinforced polymer network formed aggregates with a wide range of sizes and shapes in random directions. However, higher concentrations of nanocellulose induced brittle fracture due to the aggregation at localized points.

**3.2.3. FTIR Analysis.** Figure 4 shows the FTIR analysis of chemical functional groups of GT powder and PVA, PVA/GT, and PVA/GT/CNC films. The FTIR spectra for GT powder with an absorption band at  $2149 \text{ cm}^{-1}$  corresponded to various carbonyl groups in the gum while peaks of carbonyl stretching in aldehydes, ketones, and carboxylic acids were presented at  $1750 \text{ cm}^{-1}$  [70]. The bands at  $1635 \text{ cm}^{-1}$  and  $1442 \text{ cm}^{-1}$  were attributed to asymmetrical and symmetrical stretching of carboxylate groups, respectively, while peaks at  $1242 \text{ cm}^{-1}$  and  $1020 \text{ cm}^{-1}$  displayed C-O stretching vibration in polyols and alcoholic groups, respectively [22, 24, 25]. The band observed in all samples at  $3285 \text{ cm}^{-1}$  was characteristic of O-H stretching groups from intra- and intermolecular hydrogen bonds [15, 69] while a wider band of O-H stretching in the GT structure observed at  $3420 \text{ cm}^{-1}$  was caused by OH and COOH groups [25, 57].



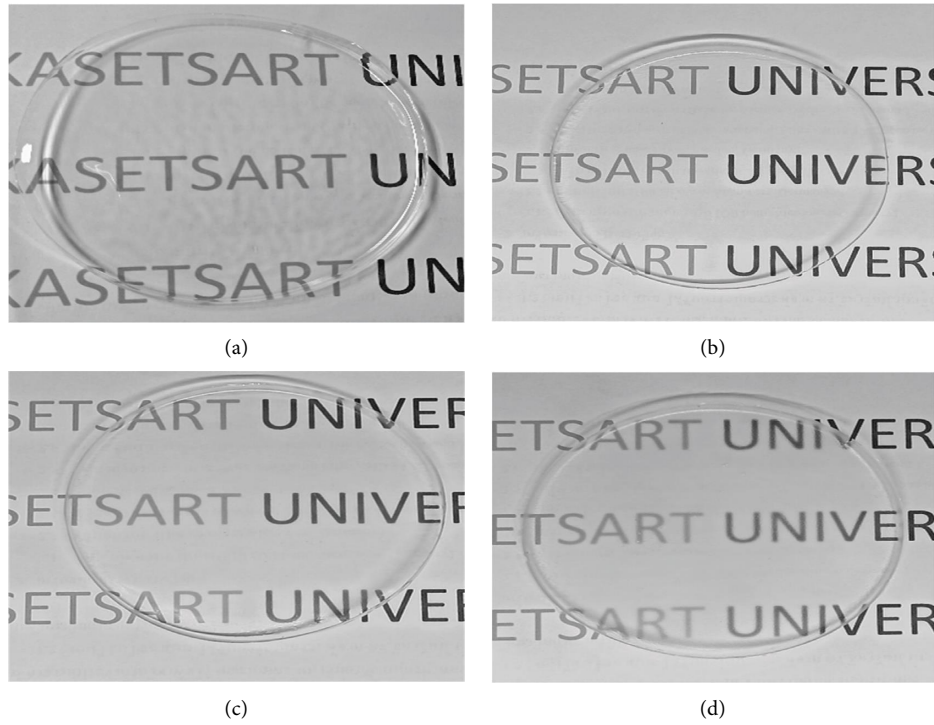


FIGURE 2: Photographs of (a) PVA, (b) PVA/GT, (c) PVA/GT/CNC2, and (d) PVA/GT/CNC10.

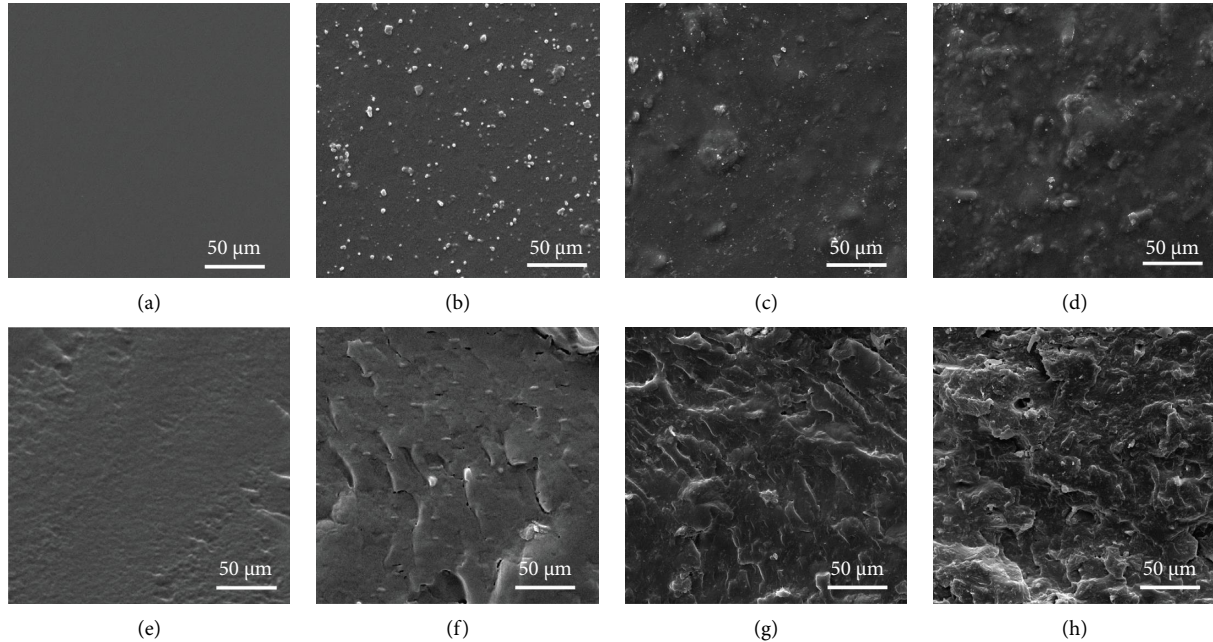


FIGURE 3: SEM micrographs of surface of (a) PVA, (b) PVA/GT, (c) PVA/GT/CNC2, and (d) PVA/GT/CNC10, and cross section of (e) PVA, (f) PVA/GT, (g) PVA/GT/CNC2, and (h) PVA/GT/CNC10 composite films.

Asymmetrical and symmetrical stretching vibrations of methylene groups were presented at  $2939\text{ cm}^{-1}$  and  $2908\text{ cm}^{-1}$ , respectively [24], while the peak at  $1086\text{ cm}^{-1}$  was assigned to C-O stretching [57, 69]. Vinyl C-H in plane bending of PVA was confirmed at  $1419\text{ cm}^{-1}$ . Furthermore,

the absorption band centered at  $842\text{ cm}^{-1}$  represented C=C bending [71, 72]. No significant changes were observed in the chemical structure of PVA after the incorporation of GT and CNCs. Notably, addition of CNCs at high concentration contributed C=C stretching at  $1655\text{ cm}^{-1}$  [73].

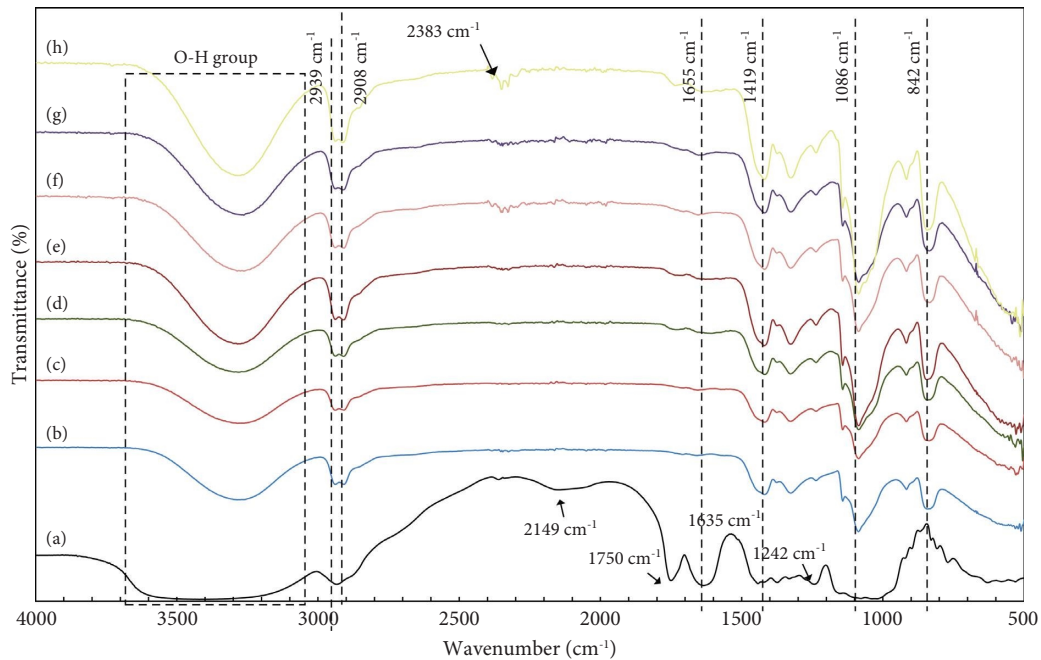


FIGURE 4: FTIR spectra of (a) GT, (b) PVA, (c) PVA/GT, (d) PVA/GT/CNC2, (e) PVA/GT/CNC4, (f) PVA/GT/CNC6, (g) PVA/GT/CNC8, and (h) PVA/GT/CNC10 composite films.

**3.2.4. Swelling Ratio of Composite Film.** Results in Figure 5 show the swelling ability of the various films. At the initial stage, the large number of free hydroxyl groups in the PVA film absorbed water molecules to reach a maximum state of approximately 260% before reducing at 1.5 h. PVA/GT films increased gradually and reached a steady rate of 250% due to the presence of hydrogen bonds in hydroxyl and carboxyl functional groups [70]. The porous structure of GT helped in trapping water molecules [20, 68, 74]. After 6 h, swelling ability slightly decreased to 230% for 7 days due to degradations in the polymer matrix [75]. There were no obvious differences in PVA/GT/CNC2 and PVA/GT films. Addition of small amounts of CNCs increased water absorption in the polymer matrix. However, as CNC concentration increased, extra swelling capacity was restrained [58, 69, 76] due to the reinforcing effects of CNCs. This reduction illustrated the hydrogen bonding between CNCs and polymers. Thus, water molecules could not freely pass through the polymer [76, 77]. The PVA/GT/CNC2 film provided swelling behavior that could create an environment suitable for wound healing [14, 17, 78, 79]. Swelling of wound dressing is an important factor that relates to wound exudate absorption and prevention of infection. This is as a result of physical and chemical changes in material structure that help water molecules to diffuse internally, leading to an increase in free volume [69, 78, 80].

**3.2.5. Stability.** Stability of the wound dressing was assessed as the percentage weight loss of composite film over a period of 7 days to indicate its prolonged use. The result in Figure 6 shows that the PVA film exhibited the highest rate of weight loss of 9.8% on the first day, which increased to 17.2% on the 7<sup>th</sup> day due to solvation and fragmentation of the film [80].

There was significant difference between the neat PVA and the composite films. The addition of GT improved the film stability by maintaining weight loss below 12% for 7 days. Bassorin fragments in GT are insoluble in water; these probably reduced the film's solubility [81]. The solubility was further reduced when CNCs were added. This could be explained as due to the formation of a strong matrix of hydrogen bonds through the three-dimensional structure of CNCs and the polymeric matrix that reduced free hydroxyl groups and restricted water penetration [58, 77].

**3.2.6. Mechanical Properties.** Mechanical properties of the films are summarized in Table 2. Wound dressing should be strong, flexible, and elastic for efficient treatment; thus, the film was evaluated in terms of tensile strength, elongation at break, and elastic modulus. The neat PVA film exhibited a tensile strength of 54.63 MPa, which reduced slightly to 49.26 MPa when GT was added. There was no significant difference ( $p < 0.05$ ) between neat PVA and PVA/GT. This result agreed with Ojagh et al. [82] who found that the addition of GT had no significant effect on mechanical properties. Highest tensile strength was recorded in PVA/GT/CNC2 (80.39 MPa), while PVA/GT/CNC6 gave the lowest strength of  $45.05 \pm 3.39$  MPa. The addition of CNCs increased the strength of the material by entrapping inside the matrix. This allowed strong hydrogen bond formation between the nanocellulose and PVA matrix, thus impacting mechanical integrity [61, 83]. However, high concentration of CNCs led to agglomeration of particles, increased rigidity, and poor distribution in polymer matrices, which affected the formation of hydrogen bonds among polymer chains and inhibited reinforcing properties [15, 71]. Elastic modulus of PVA and PVA/GT was  $1223.08 \pm 182.08$  MPa and

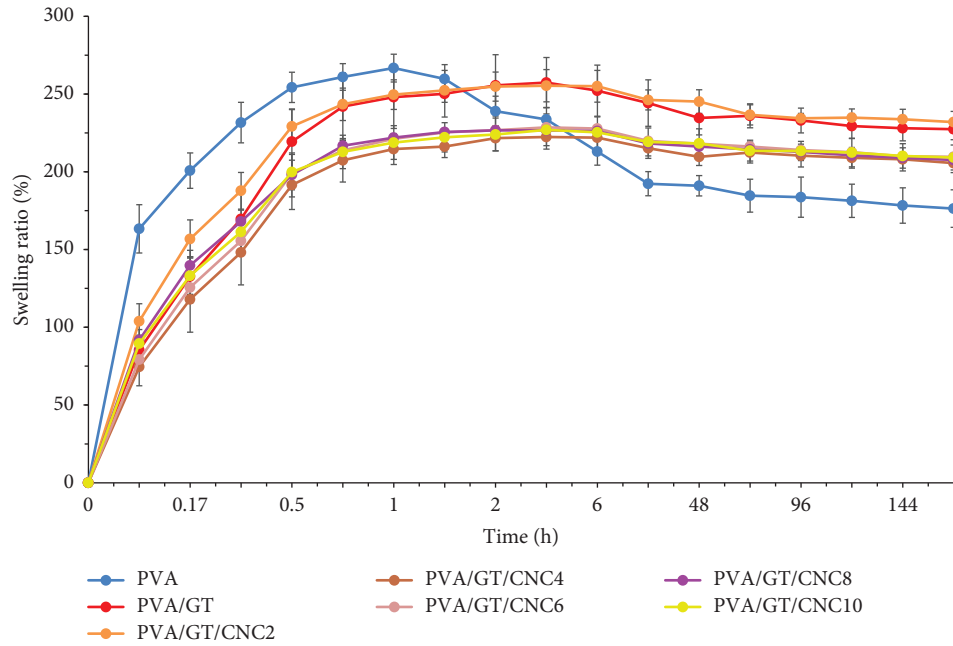


FIGURE 5: Swelling ratio of neat PVA, PVA/GT, and PVA/GT/CNC composite films.

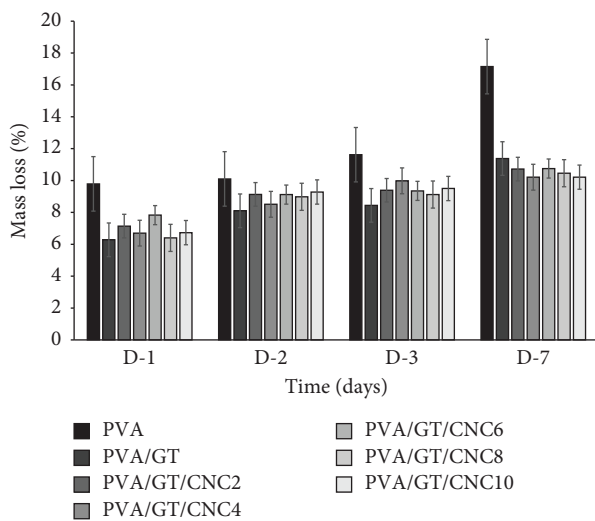


FIGURE 6: Percentage weight loss of PVA, PVA/GT, and PVA/GT/CNC composite films.

1062.51 ± 101.65 MPa, respectively. Highest elastic modulus of 1526.11 ± 31.86 MPa was recorded in the PVA/GT/CNC2 film, which decreased to 1260.45 ± 76.94 MPa in PVA/GT/CNC10. The high value was attributed to the crystalline nature of CNCs that resulted in better alignment and enhanced elastic modulus [69, 83]. There was no significant difference in elastic modulus of neat PVA and composite films loaded with CNCs, which implies the nanoparticles has no negative effect on the elastic nature of PVA. Neat PVA had elongation at break of 48.52% and this slightly decreased to 44.48% in PVA/GT. However, elongation at break of PVA/GT/CNC films decreased drastically with increasing concentration of CNCs. The elongation at break significantly

decreased to 8.11% in PVA/GT/CNC2 and dropped further to 3.92% in the PVA/GT/CNC10 film due to the rigid nature of CNCs. Since CNCs are nondeformable, strong interaction between CNCs and the polymer matrix did not allow elongation in the composite materials [84]. The tensile strength of wound dressings should be adequate for application and storage to ensure that it is not easily damaged by handling [85, 86]. Therefore, PVA/GT/CNC composite materials in the range of 45–80 MPa showed good mechanical properties compared to previous studies [86–88] for wound dressing. The stress-strain curves of PVA, PVA/GT, and PVA/GT/CNC with different concentrations of CNC are presented in Figure 7.

**3.2.7. Cytotoxicity.** The cytotoxicity of PVA, PVA/GT, and PVA/GT/CNC10 films was evaluated using the MTT assay. The sample with the highest CNC concentration (PVA/GT/CNC10) was tested to confirm nontoxicity and safety of the film for cell growth. The result in Figure 8 shows all the test samples except that the positive controls (which is expected) are nontoxic to fibroblast cells with reference to ISO 10993-5 standard with acceptable limit of 70% cell viability [59, 89]. Cell viability of PVA and PVA/GT was 93% and 84%, respectively. The decrease in cell viability of the PVA/GT film may be due to the diversity in chemical composition that slightly influenced the biological properties of the film [20]. The PVA/GT/CNC10 film, which contains high concentration of CNCs, was found to be nontoxic to fibroblast cells with 95% cell viability. The value is closer to that of the negative control of 99% cell viability. Incorporation of CNCs in the polymeric matrix and reaction between CNCs and PVA/GT improved cell viability in the films. The film satisfied noncytotoxic requirement of cell viability above 70% in agreement with previous reports [24, 89, 90].



TABLE 2: Mechanical properties of PVA/GT/CNC composite films.

Samples	Tensile strength (MPa)	Elongation at break (%)	Elastic modulus (MPa)
PVA	54.63 ± 0.69 <sup>bc</sup>	48.52 ± 1.57 <sup>a</sup>	1223.08 ± 182.08 <sup>a</sup>
PVA/GT	49.26 ± 5.00 <sup>bc</sup>	44.38 ± 5.03 <sup>a</sup>	1062.51 ± 101.65 <sup>b</sup>
PVA/GT/CNC2	80.39 ± 1.41 <sup>a</sup>	8.11 ± 0.30 <sup>b</sup>	1526.11 ± 31.86 <sup>a</sup>
PVA/GT/CNC4	59.09 ± 4.26 <sup>b</sup>	7.36 ± 0.82 <sup>b</sup>	1450.74 ± 76.94 <sup>a</sup>
PVA/GT/CNC6	45.05 ± 3.39 <sup>c</sup>	8.81 ± 1.56 <sup>b</sup>	1299.13 ± 120.37 <sup>a</sup>
PVA/GT/CNC8	47.63 ± 3.54 <sup>bc</sup>	6.88 ± 0.06 <sup>b</sup>	1353.38 ± 177.19 <sup>a</sup>
PVA/GT/CNC10	47.68 ± 9.26 <sup>bc</sup>	3.92 ± 0.92 <sup>b</sup>	1260.45 ± 76.94 <sup>a</sup>

For values with the same letter, the difference is not statistically significant, while different letters mean statistical significance ( $p \leq 0.05$ ).

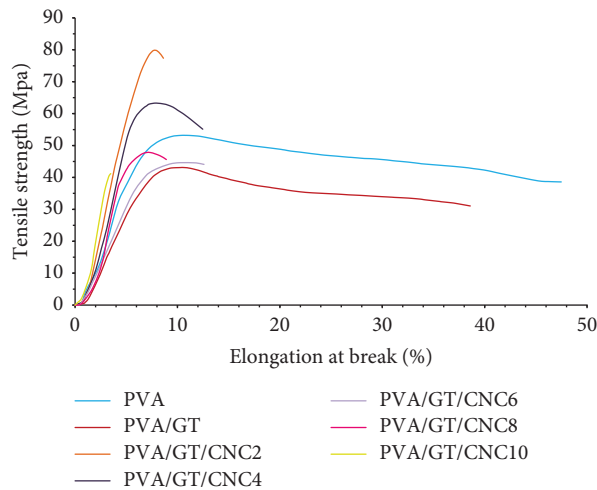


FIGURE 7: Stress-strain curves of PVA, PVA/GT, and PVA/GT/CNC with different concentrations of CNC (2 to 10%).

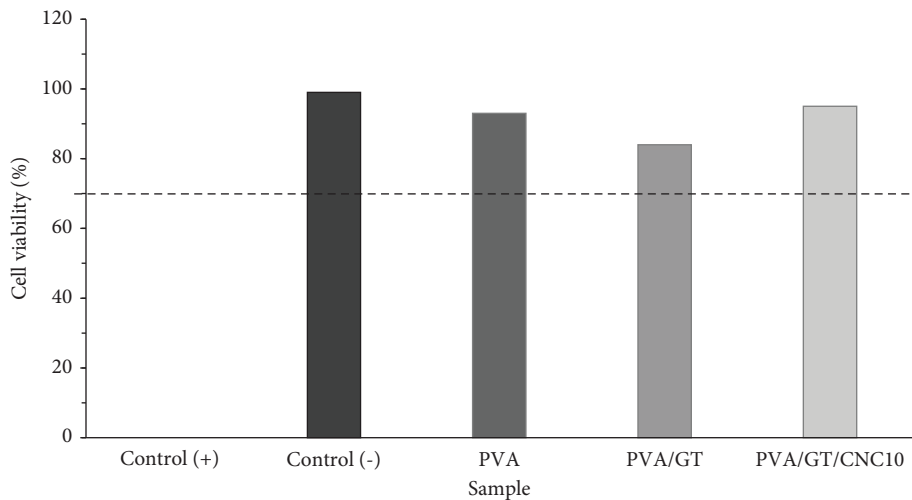


FIGURE 8: Cell viability of PVA, PVA/GT, and PVA/GT/CNC10 compared with positive and negative controls.

3.2.8. *Antibacterial Activity.* Figure 9 shows clear zones around discs, which increased with increasing concentration of the betel leaf extract. Disc diffusion result revealed that films loaded with the betel leaf extract at different concentrations of 2%, 3%, and 4%, exhibited excellent antibacterial activity against both gram-negative (*P. aeruginosa*)

and gram-positive (*S. aureus*) bacteria. There was high significant difference in inhibition zone between the positive control (erythromycin) and the films loaded with extracts (Table 3). As expected, there was no inhibition zone in the negative control. The film loaded with 4% extract (PVA/GT/CNC2\_4%) recorded the highest inhibition zone of

TABLE 3: Antimicrobial activity of PVA/GT/CNC2 film loaded with betel extract on the agar diffusion test.

Samples	Diameter of inhibition zone (mm)	
	<i>P. aeruginosa</i>	<i>S. aureus</i>
PVA/GT/CNC2_2%	16.60 ± 1.03 <sup>b</sup>	18.00 ± 0.79 <sup>b</sup>
PVA/GT/CNC2_3%	19.00 ± 1.41 <sup>b</sup>	22.00 ± 1.13 <sup>b</sup>
PVA/GT/CNC2_4%	23.60 ± 0.55 <sup>a</sup>	28.20 ± 0.84 <sup>a</sup>
Positive control	12.30 ± 0.57 <sup>c</sup>	14.40 ± 1.14 <sup>c</sup>
Negative control	—	—

For values with the same letter, the difference is not statistically significant, while different letters mean statistical significance ( $p \leq 0.05$ ).

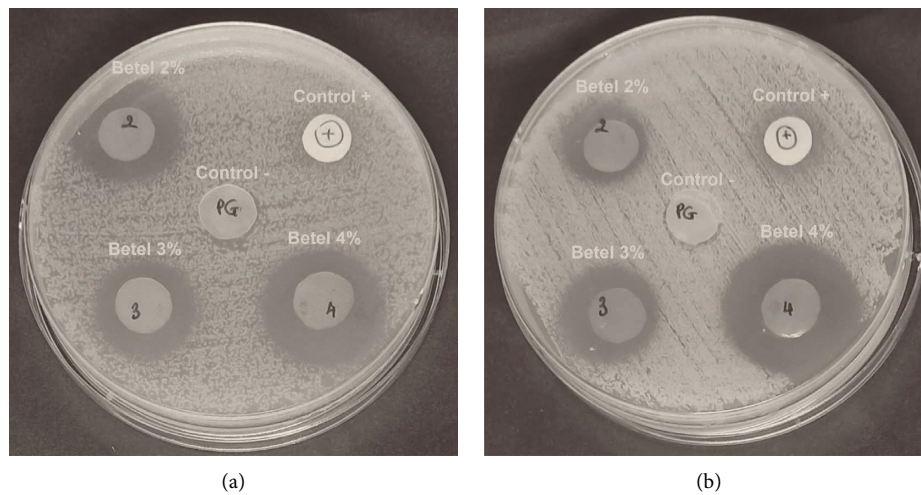


FIGURE 9: Antibacterial activity of PVA/GT/CNC2 films loaded with 2%, 3%, and 4% of crude betel extracts against *P. aeruginosa* (a) and (b) *S. aureus*.

23.60 ± 0.55 mm and 28.20 ± 0.84 mm for *P. aeruginosa* (Figure 9(a)) and *S. aureus* (Figure 9(b)), respectively. In all, *S. aureus* is more susceptible than *P. aeruginosa* which may be as a result of the differences in their cell wall structure [91, 92]. The cell wall of *S. aureus* has only peptidoglycan layer, while that of *P. aeruginosa* is made of three layers such as the inner or cytoplasmic membrane, peptidoglycan layer, and outer membrane [91, 93, 94]. The betel leaf extract contained an essential oil and phenolic compounds which are reported to inhibit bacterial cell growth [95–97]. The presence of oxygenated terpenoids including alcohols and phenolic terpenes [96] as well as hydroxyl groups in hydrophobic fatty acids and fatty acid ester components caused destabilization of the cytoplasmic membrane, disrupted proton and electron flow, and decreased adenosine triphosphate (ATP) synthesis, leading to cell death [44, 98].

#### 4. Conclusions

The PVA/GT/CNC composite film was successfully prepared as wound dressing material. The films exhibited higher swelling ratio and mechanical properties with good transparency, which are ideal for wound dressing. These properties could help to absorb exudates with easy daily observation and minimize trauma to the wound bed.

Incorporation of CNCs from 2% to 10% improved the physicochemical properties of the film. The PVA/GT/CNC2 showed excellent properties among the CNC-based composite films. Apart from the physicochemical enhancements, the cytocompatibility was also improved. The film loaded with the betel leaf extract exhibited excellent antibacterial activity against *P. aeruginosa* and *S. aureus* strains. Therefore, the prepared nanocomposite film with good features will provide the optimum conditions for wound healing, especially in cutaneous wound dressing application. The visual inspection property of PVA/GT/CNC coupled with antibacterial activity from the betel leaf extract and other excellent physicochemical characteristics of the film are suitable for wound healing application. This dressing can protect the wound surface from infection and dehydration, which deprives wound tissues of oxygen and the nutrients necessary for healing.

#### Data Availability

The data that support the findings of this study are available upon reasonable request from the corresponding author.

#### Disclosure

A preprint of this article has previously been published.

## Conflicts of Interest

The authors declare that they have no conflicts of interest.

## Acknowledgments

The authors are grateful to the Ministry of Higher Education, Science, Research and Innovation, Thailand, for the financial support. They are also grateful to the Department of Biotechnology, Faculty of Agro-Industry, and Kasetsart University for “Agro-Industry (AI) Scholarship for International Students 2018.” Supports from the Thailand-India Program of Science and Technology Cooperation and the members of Cellulose for Future Materials and Technologies Special Research Unit during various stages of the research are greatly appreciated.

## References

- [1] S. Kumbar, C. Laurencin, and M. Deng, *Natural and synthetic biomedical polymers* Newnes, Elsevier, Amsterdam, Netherlands, 2014.
- [2] A. Aravamudhan, D. M. Ramos, A. A. Nada, and S. G. Kumbar, “Chapter 4 natural polymers: polysaccharides and their derivatives for biomedical applications,” in *Natural and Synthetic Biomedical Polymers*, S. G. Kumbar, C. T. Laurencin, and M. Deng, Eds., Elsevier, Amsterdam, Netherlands, 2014.
- [3] A. Sionkowska, “Current research on the blends of natural and synthetic polymers as new biomaterials: review,” *Progress in Polymer Science*, vol. 36, no. 9, pp. 1254–1276, 2011.
- [4] S. Ghosh, P. Roy, and D. Lahiri, “Recent trends in electrospinning for the preparation of ultrathin plastic and polymer fibers for bio-medical applications,” in *Encyclopedia of Materials: Plastics and Polymers*, M. S. J. Hashmi, Ed., Elsevier, Amsterdam, Netherlands, 2022.
- [5] B. C. Simionescu and D. Ivanov, “Natural and synthetic polymers for designing composite materials,” in *Handbook of Bioceramics and Biocomposites*, I. V. Antoniac, Ed., Springer International Publishing, Berlin, Germany, 2014.
- [6] L. Xu, Y. Li, S. Gao et al., “Preparation and properties of cyanobacteria-based carbon quantum dots/polyvinyl alcohol/nanocellulose composite,” *Polymers*, vol. 12, no. 5, p. 1143, 2020.
- [7] N. Usawattanakul, S. Torgbo, P. Sukyai, S. Khantayanuwong, B. Puangsin, and P. Srichola, “Development of nanocomposite film comprising of Polyvinyl Alcohol (PVA) incorporated with bacterial cellulose nanocrystals and magnetite nanoparticles,” *Polymers*, vol. 13, no. 11, p. 1778, 2021.
- [8] M. Aslam, M. A. Kalyar, and Z. A. Raza, “Polyvinyl alcohol: a review of research status and use of polyvinyl alcohol based nanocomposites,” *Polymer Engineering & Science*, vol. 58, no. 12, pp. 2119–2132, 2018.
- [9] M. Teodorescu, M. Bercea, and S. Morariu, “Biomaterials of PVA and PVP in medical and pharmaceutical applications: perspectives and challenges,” *Biotechnology Advances*, vol. 37, no. 1, pp. 109–131, 2019.
- [10] I. Yadav, V. S. Rathnam, Y. Yogalakshmi et al., “Synthesis and characterization of polyvinyl alcohol- carboxymethyl tamarind gum based composite films,” *Carbohydrate Polymers*, vol. 165, pp. 159–168, 2017.
- [11] D. Zhang, W. Zhou, B. Wei et al., “Carboxyl-modified poly(vinyl alcohol)-crosslinked chitosan hydrogel films for potential wound dressing,” *Carbohydrate Polymers*, vol. 125, pp. 189–199, 2015.
- [12] S.-P. Lin, K.-Y. Lo, T.-N. Tseng, J.-M. Liu, T.-Y. Shih, and K.-C. Cheng, “Evaluation of PVA/dextran/chitosan hydrogel for wound dressing,” *Cellular Polymers*, vol. 38, no. 1-2, pp. 15–30, 2019.
- [13] C. Zheng, C. Liu, H. Chen et al., “Effective wound dressing based on Poly (vinyl alcohol)/Dextran-aldehyde composite hydrogel,” *International Journal of Biological Macromolecules*, vol. 132, pp. 1098–1105, 2019.
- [14] H. Fang, J. Wang, L. Li et al., “A novel high-strength poly(ionic liquid)/PVA hydrogel dressing for antibacterial applications,” *Chemical Engineering Journal*, vol. 365, pp. 153–164, 2019.
- [15] K. Choo, Y. C. Ching, C. H. Chuah, S. Julai, and N. S. Liou, “Preparation and characterization of polyvinyl alcohol-chitosan composite films reinforced with cellulose nanofiber,” *Materials*, vol. 9, no. 8, p. 644, 2016.
- [16] F. Wahid, F. P. Wang, Y. Y. Xie et al., “Reusable ternary PVA films containing bacterial cellulose fibers and epsilon-polylysine with improved mechanical and antibacterial properties,” *Colloids and Surfaces B: Biointerfaces*, vol. 183, Article ID 110486, 2019.
- [17] P. P. Patil, R. A. Bohara, J. V. Meshram, S. G. Nanaware, and S. H. Pawar, “Hybrid chitosan-ZnO nanoparticles coated with a sonochemical technique on silk fibroin-PVA composite film: a synergistic antibacterial activity,” *International Journal of Biological Macromolecules*, vol. 122, pp. 1305–1312, 2019.
- [18] M. Ranjbar-Mohammadi, M. P. Prabhakaran, S. H. Bahrami, and S. Ramakrishna, “Gum tragacanth/poly(L-lactic acid) nanofibrous scaffolds for application in regeneration of peripheral nerve damage,” *Carbohydrate Polymers*, vol. 140, pp. 104–112, 2016.
- [19] S. Ahmad, M. Ahmad, K. Manzoor, R. Purwar, and S. Ikram, “A review on latest innovations in natural gums based hydrogels: preparations & applications,” *International Journal of Biological Macromolecules*, vol. 136, pp. 870–890, 2019.
- [20] E. Nazarzadeh Zare, P. Makvandi, and F. R. Tay, “Recent progress in the industrial and biomedical applications of tragacanth gum: a review,” *Carbohydrate Polymers*, vol. 212, pp. 450–467, 2019.
- [21] M. E. Taghavizadeh Yazdi, S. Nazarnezhad, S. H. Mousavi et al., “Gum tragacanth (GT): a versatile biocompatible material beyond borders,” *Molecules*, vol. 26, no. 6, p. 1510, 2021.
- [22] M. Abdoli, K. Sadrjavadi, E. Arkan et al., “Polyvinyl alcohol/Gum tragacanth/graphene oxide composite nanofiber for antibiotic delivery,” *Journal of Drug Delivery Science and Technology*, vol. 60, Article ID 102044, 2020.
- [23] D. Qureshi, K. P. Behera, D. Mohanty et al., “Synthesis of novel poly (vinyl alcohol)/tamarind gum/bentonite-based composite films for drug delivery applications,” *Colloids and Surfaces A: Physicochemical and Engineering Aspects*, vol. 613, Article ID 126043, 2021.
- [24] Z. Zarekhalili, S. H. Bahrami, M. Ranjbar-Mohammadi, and P. B. Milan, “Fabrication and characterization of PVA/Gum tragacanth/PCL hybrid nanofibrous scaffolds for skin substitutes,” *International Journal of Biological Macromolecules*, vol. 94, pp. 679–690, 2017.
- [25] M. Ranjbar-Mohammadi, S. H. Bahrami, and M. T. Joghataei, “Fabrication of novel nanofiber scaffolds from gum tragacanth/poly(vinyl alcohol) for wound dressing application:

- in vitro evaluation and antibacterial properties,” *Materials Science and Engineering: C*, vol. 33, no. 8, pp. 4935–4943, 2013.
- [26] B. Singh, L. Varshney, S. Francis, and Rajneesh, “Designing tragacanth gum based sterile hydrogel by radiation method for use in drug delivery and wound dressing applications,” *International Journal of Biological Macromolecules*, vol. 88, pp. 586–602, 2016.
- [27] M. Ranjbar Mohammadi, S. Kargozar, S. H. Bahrami, and S. Rabbani, “An excellent nanofibrous matrix based on gum tragacanth-poly (E-caprolactone)-poly (vinyl alcohol) for application in diabetic wound healing,” *Polymer Degradation and Stability*, vol. 174, Article ID 109105, 2020.
- [28] Z. Doozandeh, S. Saber-Samandari, and A. Khandan, “Preparation of novel Arabic gum-C6H9NO biopolymer as a bed sore for wound care application,” *Acta Medica Iranica*, vol. 34, pp. 520–530, 2020.
- [29] H. A. Heydari, E. Karamian, E. Poorazizi, A. Khandan, and J. Heydaripour, “A novel nano-fiber of Iranian gum tragacanth-polyvinyl alcohol/nanoclay composite for wound healing applications,” *Procedia Materials Science*, vol. 11, pp. 176–182, 2015.
- [30] M. Darroudi, M. Sarani, R. Kazemi Oskuee, A. Khorsand Zak, and M. S. Amiri, “Nanoceria: gum mediated synthesis and in vitro viability assay,” *Ceramics International*, vol. 40, no. 2, pp. 2863–2868, 2014.
- [31] M. Chantaso, K. Chaiyong, R. Meesupthong et al., “Sugarcane leave-derived cellulose nanocrystal/graphene oxide filter membrane for efficient removal of particulate matter,” *International Journal of Biological Macromolecules*, vol. 234, Article ID 123676, 2023.
- [32] S. Torgbo, V. M. Quan, and P. Sukyai, “Cellulosic value-added products from sugarcane bagasse,” *Cellulose*, vol. 28, no. 9, pp. 5219–5240, 2021.
- [33] P. Singh, P. Singh, and J. Singh, “Sugarcane bagasse: a potential and economical source for raising sugarcane nursery in sub-tropical India,” *Sugar Tech*, vol. 23, no. 6, pp. 1211–1217, 2021.
- [34] R. Z. Khoo, W. S. Chow, and H. Ismail, “Sugarcane bagasse fiber and its cellulose nanocrystals for polymer reinforcement and heavy metal adsorbent: a review,” *Cellulose*, vol. 25, no. 8, pp. 4303–4330, 2018.
- [35] H. Du, W. Liu, M. Zhang, C. Si, X. Zhang, and B. Li, “Cellulose nanocrystals and cellulose nanofibrils based hydrogels for biomedical applications,” *Carbohydrate Polymers*, vol. 209, pp. 130–144, 2019.
- [36] A. B. Seabra, J. S. Bernardes, W. J. Favaro, A. J. Paula, and N. Duran, “Cellulose nanocrystals as carriers in medicine and their toxicities: a review,” *Carbohydrate Polymers*, vol. 181, pp. 514–527, 2018.
- [37] T. Aziz, A. Ullah, H. Fan et al., “Cellulose nanocrystals applications in health, medicine and catalysis,” *Journal of Polymers and the Environment*, vol. 29, no. 7, pp. 2062–2071, 2021.
- [38] M.-C. Popescu, B.-I. Dogaru, and C.-M. Popescu, “Effect of cellulose nanocrystals nanofiller on the structure and sorption properties of carboxymethyl cellulose-glycerol-cellulose nanocrystals nanocomposite systems,” *Materials*, vol. 13, no. 13, p. 2900, 2020.
- [39] Y. Hussein, E. M. El-Fakharany, E. A. Kamoun et al., “Electrospun PVA/hyaluronic acid/L-arginine nanofibers for wound healing applications: nanofibers optimization and in vitro bioevaluation,” *International Journal of Biological Macromolecules*, vol. 164, pp. 667–676, 2020.
- [40] F. Avila-Salas, A. Marican, S. Pinochet et al., “Film dressings based on hydrogels: simultaneous and sustained-release of bioactive compounds with wound healing properties,” *Pharmaceutics*, vol. 11, no. 9, p. 447, 2019.
- [41] A. Gaspar-Pintilieșcu, A.-M. Stanciu, and O. Craciunescu, “Natural composite dressings based on collagen, gelatin and plant bioactive compounds for wound healing: a review,” *International Journal of Biological Macromolecules*, vol. 138, pp. 854–865, 2019.
- [42] A. Amalraj, K. K. J. Raj, J. T. Haponiuk, S. Thomas, and S. Gopi, “Preparation, characterization, and antimicrobial activity of chitosan/gum Arabic/polyethylene glycol composite films incorporated with black pepper essential oil and ginger essential oil as potential packaging and wound dressing materials,” *Advanced Composites and Hybrid Material*, vol. 3, no. 4, pp. 485–497, 2020.
- [43] O. Asanarong, V. Minh Quan, S. Boonrungsiman, and P. Sukyai, “Bioactive wound dressing using bacterial cellulose loaded with papain composite: morphology, loading/release and antibacterial properties,” *European Polymer Journal*, vol. 143, Article ID 110224, 2021.
- [44] R. A. Umar, N. A. Sanusi, M. N. Zahary, M. A. K. Rohin, and S. Ismail, “Chemical composition and the potential biological activities of piper betel a review,” *Malaysian Journal of Applied Sciences*, vol. 3, no. 1, p. 8, 2018.
- [45] M. Madhumita, P. Guha, and A. Nag, “Bio-actives of betel leaf (Piper betle L.): a comprehensive review on extraction, isolation, characterization, and biological activity,” *Phytotherapy Research*, vol. 22, 2020.
- [46] A. Datta, S. Ghoshdastidar, and M. Singh, “Antimicrobial property of piper betel leaf against clinical isolates of bacteria,” *International Journal of Pharma Sciences and Research*, vol. 2, no. 3, p. 6, 2011.
- [47] V. Dwivedi and S. Tripathi, “Review study on potential activity of Piper betle,” *Journal of Pharmacognosy and Phytochemistry*, vol. 3, no. 4, p. 6, 2014.
- [48] U. Taukoorah, N. Lall, and F. Mahomoodally, “Piper betle L. (betel quid) shows bacteriostatic, additive, and synergistic antimicrobial action when combined with conventional antibiotics,” *South African Journal of Botany*, vol. 105, pp. 133–140, 2016.
- [49] D. Ilenghoven, C. Y. Chan, W. Wan Ahmad Kamal, S. MohdYussof, and S. Ibrahim, “A review of wound dressing practices,” *Clinical Dermatology Open Access Journal*, vol. 2, no. 6, 2017.
- [50] L. Jun, S. Lichun, L. Ping et al., “The wound dressings and their applications in wound healing and management,” *Health Science*, vol. 13, no. 4, 2019.
- [51] L. N. Diem, I. Banerjee, K. Pal, U. Sukatta, P. Rugthaworn, and P. Sukyai, *Evaluation in Cellulose Nanocrystals Effectiveness on Composite Film Based Wound Dressing from Poly (Vinyl Alcohol) and Gum Tragacanth*, Kasetsart University, Bangkok, Thailand, 2021.
- [52] G. J. M. Rocha, A. R. Gonçalves, B. R. Oliveira, E. G. Olivares, and C. E. V. Rossell, “Steam explosion pretreatment re-production and alkaline delignification reactions performed on a pilot scale with sugarcane bagasse for bioethanol production,” *Industrial Crops and Products*, vol. 35, no. 1, pp. 274–279, 2012.
- [53] N. T. Lam, W. Saewong, and P. Sukyai, “Effect of varying hydrolysis time on extraction of spherical bacterial cellulose nanocrystals as a reinforcing agent for poly(vinyl alcohol) composites,” *Journal of Polymer Research*, vol. 24, no. 5, p. 71, 2017.



- [54] P. Sukyai, P. Anongjanya, N. Bunyahwuthakul et al., "Effect of cellulose nanocrystals from sugarcane bagasse on whey protein isolate-based films," *Food Research International*, vol. 107, pp. 528–535, 2018.
- [55] N. Imchalee, R. Meesupthong, S. Torgbo, and P. Sukyai, "Cellulose nanocrystals as sustainable material for enhanced painting efficiency of watercolor paint," *Surfaces and Interfaces*, vol. 27, Article ID 101570, 2021.
- [56] G. Vanitjinda, T. Nimchua, and P. Sukyai, "Effect of xylanase-assisted pretreatment on the properties of cellulose and regenerated cellulose films from sugarcane bagasse," *International Journal of Biological Macromolecules*, vol. 122, pp. 503–516, 2019.
- [57] F. S. Mostafavi, R. Kadkhodae, B. Emadzadeh, and A. Koocheki, "Preparation and characterization of tragacanth-locust bean gum edible blend films," *Carbohydrate Polymers*, vol. 139, pp. 20–27, 2016.
- [58] M.-C. Popescu, B.-I. Dogaru, and C.-M. Popescu, "The influence of cellulose nanocrystals content on the water sorption properties of bio-based composite films," *Materials and Design*, vol. 132, pp. 170–177, 2017.
- [59] P. L. Simon, "Cancer cell culture: methods and protocols," *Methods in Molecular Medicine*, vol. 88, 2004.
- [60] R. Chollakup, W. Kongtud, U. Sukatta et al., "Eco-friendly rice straw paper coated with longan (*Dimocarpus Longan*) peel extract as bio-based and antibacterial packaging," *Polymers*, vol. 13, no. 18, p. 3096, 2021.
- [61] N. Lam, R. Chollakup, W. Smitthipong, T. Nimchua, and P. Sukyai, *Characterization of Cellulose Nanocrystals Extracted from Sugarcane Bagasse for Potential Biomedical Materials*, Springer, Berlin, Germany, 2017.
- [62] R. Meesupthong, N. Yingkamhaeng, T. Nimchua et al., "Xylanase pretreatment of energy cane enables facile cellulose nanocrystal isolation," *Cellulose*, vol. 28, no. 2, pp. 799–812, 2020.
- [63] K. S. Silva, M. A. Mauro, M. P. Gonçalves, and C. M. R. Rocha, "Synergistic interactions of locust bean gum with whey proteins: effect on physicochemical and microstructural properties of whey protein-based films," *Food Hydrocolloids*, vol. 54, pp. 179–188, 2016.
- [64] L. Chen, H. Yu, M. Dirican et al., "Highly transparent and colorless nanocellulose/polyimide substrates with enhanced thermal and mechanical properties for flexible OLED displays," *Advanced Materials Interfaces*, vol. 7, Article ID 20010, 2020.
- [65] B. Tonyali, S. Cikrikci, and M. H. Oztop, "Physicochemical and microstructural characterization of gum tragacanth added whey protein based films," *Food Research International*, vol. 105, pp. 1–9, 2018.
- [66] M. Kuddushi, A. A. Shah, C. Ayranci, and X. Zhang, "Recent advances in novel materials and techniques for developing transparent wound dressings," *Journal of Materials Chemistry B*, vol. 18, 2023.
- [67] G. Xie, N. Zhou, S. Du et al., "Transparent photothermal hydrogels for wound visualization and accelerated healing," *Fundamental Research*, vol. 2, no. 2, pp. 268–275, 2022.
- [68] D. Khodaei, K. Oltrogge, and Z. Hamidi-Esfahani, "Preparation and characterization of blended edible films manufactured using gelatin," *Tragacanth Gum and Persian Gum*, vol. 13, 2019.
- [69] Z. Jahan, M. B. K. Niazi, and Ø. W. Gregersen, "Mechanical, thermal and swelling properties of cellulose nanocrystals/PVA nanocomposites membranes," *Journal of Industrial and Engineering Chemistry*, vol. 57, pp. 113–124, 2018.
- [70] A. Kurt, "Physicochemical, rheological and structural characteristics of alcohol precipitated fraction of gum tragacanth," *Food and Health*, pp. 183–193, 2018.
- [71] A. Mandal and D. Chakrabarty, "Characterization of nanocellulose reinforced semi-interpenetrating polymer network of poly(vinyl alcohol) & polyacrylamide composite films," *Carbohydrate Polymers*, vol. 134, pp. 240–250, 2015.
- [72] M. A. Abureesh, A. A. Oladipo, and M. Gazi, "Facile synthesis of glucose-sensitive chitosan-poly(vinyl alcohol) hydrogel: drug release optimization and swelling properties," *International Journal of Biological Macromolecules*, vol. 90, pp. 75–80, 2016.
- [73] A. B. D. Nandiyanto, R. Oktiani, and R. Ragadhita, "How to read and interpret FTIR spectroscopy of organic material," *Indonesian Journal of Science and Technology*, vol. 4, no. 1, p. 97, 2019.
- [74] K. M. Rao, A. Kumar, K. S. V. Krishna Rao, A. Haider, and S. S. Han, "Biodegradable tragacanth gum based silver nanocomposite hydrogels and their antibacterial evaluation," *Journal of Polymers and the Environment*, vol. 26, no. 2, pp. 778–788, 2017.
- [75] M. Tavakol, E. Vasheghani-Farahani, M. Soleimani, M. A. Mohammadifar, S. Hashemi-Najafabadi, and M. Hafizi, "Synthesis and characterization of an enzyme mediated in situ forming hydrogel based on gum tragacanth for biomedical applications," *Iranian Journal of Biotechnology*, vol. 12, no. 1, 2014.
- [76] A. Sutka, A. Sutka, S. Gaidukov, M. Timusk, J. Gravitis, and S. Kukle, "Enhanced stability of PVA electrospun fibers in water by adding cellulose nanocrystals," *Holzforschung*, vol. 69, no. 6, pp. 737–743, 2015.
- [77] A. M. Slavutsky and M. A. Bertuzzi, "Water barrier properties of starch films reinforced with cellulose nanocrystals obtained from sugarcane bagasse," *Carbohydrate Polymers*, vol. 110, pp. 53–61, 2014.
- [78] M. Sadat Hosseini, K. Hemmati, and M. Ghaemy, "Synthesis of nanohydrogels based on tragacanth gum biopolymer and investigation of swelling and drug delivery," *International Journal of Biological Macromolecules*, vol. 82, pp. 806–815, 2016.
- [79] X. Zhao, H. Wu, B. Guo, R. Dong, Y. Qiu, and P. X. Ma, "Antibacterial anti-oxidant electroactive injectable hydrogel as self-healing wound dressing with hemostasis and adhesiveness for cutaneous wound healing," *Biomaterials*, vol. 122, pp. 34–47, 2017.
- [80] A. Kumar, Y. S. Negi, V. Choudhary, and N. K. Bhardwaj, "Microstructural and mechanical properties of porous biocomposite scaffolds based on polyvinyl alcohol, nano-hydroxyapatite and cellulose nanocrystals," *Cellulose*, vol. 21, no. 5, pp. 3409–3426, 2014.
- [81] S. Pirsá, F. Mohtarami, and S. Kalantari, "Preparation of biodegradable composite starch/tragacanth gum/Nanoclay film and study of its physicochemical and mechanical properties," *Chemical Review and Letters*, vol. 3, p. 9, 2020.
- [82] S. M. Ojagh, F. Shariatmadari, A. Adeli, M. Kordjazi, and M. Abdollahi, "Preparation of chitosan/tragacanth composite film and evaluation of its mechanical and physical properties," *Innovative Food Technologies*, vol. 4, no. 3, p. 10, 2017.
- [83] X. Sun, Q. Wu, X. Zhang et al., "Nanocellulose films with combined cellulose nanofibers and nanocrystals: tailored thermal, optical and mechanical properties," *Cellulose*, vol. 25, no. 2, pp. 1103–1115, 2017.
- [84] Y. C. Ching, A. Rahman, K. Y. Ching, N. L. Sukiman, and H. C. Cheng, "Preparation and characterization of polyvinyl

- alcohol- based composite reinforced with nanocellulose and nanosilica,” *Bioresources*, vol. 10, no. 2, 2015.
- [85] J. J. Elsner, A. Kraitzer, O. Grinberg, and M. Zilberman, “Highly porous drug-eluting structures: from wound dressings to stents and scaffolds for tissue regeneration,” *Biomatter*, vol. 2, no. 4, pp. 239–270, 2012.
- [86] A. L. R. Pires and Â. M. Moraes, “Improvement of the mechanical properties of chitosan-alginate wound dressings containing silver through the addition of a biocompatible silicone rubber,” *Journal of Applied Polymer Science*, vol. 24, 2014.
- [87] W. Y. Tong, A. Y. K. bin Abdullah, N. A. S. binti Rozman et al., “Antimicrobial wound dressing film utilizing cellulose nanocrystal as drug delivery system for curcumin,” *Cellulose*, vol. 25, no. 1, pp. 631–638, 2017.
- [88] M. Schoeler, F. Scremin, N. de Mendonça et al., “Cellulose nanofibers from cassava agro-industrial waste as reinforcement in pva films,” *Química Nova*, 2020.
- [89] M.-J. Buer Boyetey, S. Torgbo, P. Sukyai, N. Watthanasakphuban, and N. Kamonsutthipajit, “Filter cake-derived calcium carbonate polymorphs from sugar refinery for hydroxyapatite production as a sustainable material for biomedical application,” *Ceramics International*, vol. 49, no. 14, pp. 23417–23425, 2023.
- [90] N. T. Lam, R. Chollakup, W. Smitthipong, T. Nimchua, and P. Sukyai, “Utilizing cellulose from sugarcane bagasse mixed with poly(vinyl alcohol) for tissue engineering scaffold fabrication,” *Industrial Crops and Products*, vol. 100, pp. 183–197, 2017.
- [91] B. Jonsirivilai, S. Torgbo, and P. Sukyai, “Multifunctional filter membrane for face mask using bacterial cellulose for highly efficient particulate matter removal,” *Cellulose*, vol. 29, no. 11, pp. 6205–6218, 2022.
- [92] T. Vachanont, S. Torgbo, and P. Sukyai, “Release kinetic Model and antimicrobial activity of freeze-dried curcumin-loaded bacterial nanocellulose composite,” *Polymer Science Series A*, vol. 62, no. 3, pp. 218–227, 2020.
- [93] M. E. Arias, J. D. Gomez, N. M. Cudmani, M. A. Vattuone, and M. I. Isla, “Antibacterial activity of ethanolic and aqueous extracts of *Acacia aroma* Gill. ex Hook et Arn,” *Life Sciences*, vol. 75, no. 2, pp. 191–202, 2004.
- [94] B. H. Iglewski, “Chapter 27 pseudomonas,” *Medical Microbiology*, University of Texas Medical Branch at Galveston, Galveston, Texas, 4 edition, 1996.
- [95] N. M. D. M. W. Nayaka, M. M. V. Sasadara, D. A. Sanjaya et al., “Piper betle (L): recent review of antibacterial and antifungal properties, safety profiles, and commercial applications,” *Molecules*, vol. 26, no. 8, p. 2321, 2021.
- [96] M. Madhumita, P. Guha, and A. Nag, “Extraction of betel leaves (Piper betle L.) essential oil and its bio-actives identification: process optimization, GC-MS analysis and antimicrobial activity,” *Industrial Crops and Products*, vol. 138, Article ID 111578, 2019.
- [97] P. Guha and S. Nandi, “Essential oil of betel leaf (piper betle L.): a novel addition to the world food sector,” in *Essential Oil Research: Trends in Biosynthesis, Analytics, Industrial Applications and Biotechnological Production*, S. Malik, Ed., Springer International Publishing, Berlin, Germany, 2019.
- [98] L. Nouri and A. Mohammadi Nafchi, “Antibacterial, mechanical, and barrier properties of sago starch film incorporated with Betel leaves extract,” *International Journal of Biological Macromolecules*, vol. 66, pp. 254–259, 2014.